Interactive simulation of one-dimensional flexible parts

Mireille Grégoire and Elmar Schömer [a,b]

[a]

DaimlerChrysler Research and Technology

[b]

Johannes Gutenberg Universität Mainz, Germany

Abstract

In this paper, we present a system for simulating one dimensional flexible parts such as cables or hoses. The modeling of bending and torsion follows the Cosserat model. For this purpose we use a generalized spring-mass system and describe its configuration by a carefully chosen set of coordinates. Gravity and contact forces as well as the forces responsible for length conservation are expressed in Cartesian coordinates. But bending and torsion effects can be dealt with more effectively by using quaternions to represent the orientation of the segments joining two neighboring mass points. This augmented system allows an easy formulation of all interactions with the best appropriate coordinate type and yields a strongly banded Hessian matrix. An energy minimizing process accounts for a solution exempt from the oscillations that are typical of spring-mass systems. The whole system is numerically stable and can be solved at interactive frame rates. It is integrated in a Virtual Reality Software for use in applications such as cable routing and assembly simulation.

Key words: Cable simulation, Cosserat model, Modelling of torsion

1 Introduction

The automotive industry aims to reduce development costs and time while meeting the demand for quality and for an increasing model range. In order to meet this challenge, more and more work is done digitally. Styling reviews, Digital Mock Ups and assembly simulations are used at an early stage in the development process. Thus, potential problems can be detected and solved much earlier, long before

Email addresses: mireille.gregoire@daimlerchrysler.com, schoemer@informatik.uni-mainz.de (Mireille Grégoire and Elmar Schömer).

the first physical prototype is built. Assembly simulation is one of the applications used in the construction design process: the virtual prototype is tested and optimized for feasibility and ease of assembly. Like in other Virtual Reality applications, the physical behavior of the components needs to be simulated: collisions must be detected and contact forces must be calculated to impede the interpenetration of objects and to make them slide on each other when collisions occur. Our work is based on the Virtual Reality software *veo*, developed by DaimlerChrysler Research and Technologies, which already has a real-time collision detection and interactive contact simulation [1] as well as a real-time multibody dynamics [2]. This software had to treat flexible parts as rigid bodies, however, because it did not have a realistic way of dealing with flexible bodies.This implies that deformations that can occur in the physical world cannot be simulated, which limits the possibilities of the tool. A typical example of this would be an assembly simulation in which a cable should be pushed slightly aside to permit the mounting of another part. Studies from the business units show that most of the problems concerning flexible parts are encountered with cables, wire harnesses and hoses. These parts are also involved in another particular application: the routing. On the one hand wire harnesses are becoming more and more complex as the use of electrical and electronic components in vehicles grows; on the other hand they often need to be modified to accommodate for changes in surrounding parts or for optimization. To meet the interests of the business units, we have chosen to first concentrate on simulating these parts since they cover the most urgent need. For these bodies, one of their dimension (the length) is much bigger than the other two and their centerline contains most of the information needed to represent them. This one-dimensional nature leads to simplifications in the simulation compared to other objects such as flexible surfaces or bodies.

1.1 Previous work

Several approaches have been used for simulating various types of flexible bodies. We focus in particular on one-dimensional bodies, where the spectrum of solutions ranges from purely graphical representation of oscillations without any physics and with very low computational requirements [3] to a complete finite element simulation, such as has been used to predict the mechanical properties of cloth [4]. The domains which have contributed to the simulation of flexible parts are as diverse as the flexible parts themselves: hair and cloth simulation (see [5] and [6] for a survey on hair simulation and [7] for a survey on cloth simulation) for use in computer graphics, thread simulation for surgical training or laparoscopy, assembly simulation tools... Among the most popular computational models are differential equations [8], chains of rigid bodies [9] or spring-mass systems [10]. Mass-spring systems are a versatile way of simulating deformations and have been used for simulating a variety of flexible parts. [11] use a triangular mesh for modeling cloth. [10] implements a cable as a spring-mass model with stiff linear springs for the length conservation and torsion springs (the energy is proportional to the angle between two segments) for the bending. Hergenröther [9] models a cable as a chain of cylinder segments connected by ball joints. The chain at first has two segments and is iteratively refined, doubling the number of segments at each iteration, thus giving an inexact but fast dynamic simulation and a more exact, slower static one. [12] implements an impulse-based simulation for cables: impulses are applied at the beginning of each time-step for ensuring that the constraints are enforced in the rigid-body chain. [13] uses Geometrically Exact Dynamic Splines for modeling cables. Suturing ropes are simulated in [14] with a *Follow the Leader* algorithm: after a node has been moved to its new position, its neighbors are then moved along the line joining their old position to the new position of the moved node so that they are at the correct distance from the grasped node. The other nodes are then moved iteratively. In the case of contradictory moving directions (there are two grasped nodes, or collisions..), the resulting displacement is an average of the displacement induced by each of the constraints, which do not necessarily preserve the constraints, but the inaccuracies are not visually noticeable and are averaged out after a few iterations.

Few approaches deal with torsion. This is unfortunate, since, as shown for example in [15], torsion plays a crucial part in the deformation of a cable. One of the most interesting approaches taking the torsion into account is the one from Pai [8]. He uses a Cosserat model as a base for the simulation of suture strands during laparoscopic surgery. These strands are objects visually well approximated by a curve but nevertheless present three-dimensional body properties like twisting. In the typical use case in surgery simulation, the position and direction of the strand are defined at one end (corresponding to the end fixed in human tissues) and the forces and moments are defined at the other end, corresponding to the needle haptic device. The ordinary differential equation resulting from the Cosserat model is integrated in two passes to calculate all the variables. Another implementation of this model can be found in [16] and [17] for modeling hair. Each master strand is discretized as a smooth sequence of helical segments. The variables are then the constant curvatures and torsions of those segments. The shape of the strand can be calculated by integration. The system can be solved either by energy-minimization [16] or dynamically with a Lagrangian formulation [17]. A similar formulation, using also the curvatures and torsion as variables can be found in [18] for path-planning techniques.

1.2 Specific contributions

Being aware of the importance of torsion for the deformations of a cable, it became one of our main interests. After several attempts, we have finally chosen a generalized spring-mass system for modeling the cables. This system uses a mixed coordinate system that contains at the same time ordinary position coordinates and quaternions representing the orientation of segments on the basis of which the torsion is easy to calculate. For enforcing constraints like the conservation of length, we introduce an integral force analogous to the action of a proportional-integral controller.

2 The Cosserat model for rods

The Cosserat model for rod-like solids (with one dimension - the length - much greater than the other two cross-section dimensions) is a model from continuum mechanics. It models such a three-dimensional body as a one-dimensional one while taking into account the properties of the cross-section. A rod is then represented by its centerline (a curve in the usual three-dimensional space) associated to frames (whose vectors are the so-called directors) which represent material orientation and deformation. Such a model is well suited for real-time applications since it has a smaller number of variables (compared to finite elements models for example) and can nevertheless take into account a great number of physical properties. Large deformations are neither a problem since all the properties of the system can be defined relatively to the local frames.

2.1 Description

We consider only unstretchable and unshearable bodies (which represent the vast majority of objects of interest in the context of automotive construction). We furthermore assume that the cross-section is homogeneous and undeformable, and that the mechanical properties are constant along the length of the cable. The general Cosserat model without the above mentioned restrictions is explained in [19] or in [20]. A cable of length L is parameterized by its arc length s. It is described by a function associating to each point of the centerline of a reference configuration (generally a state without tensions like for example a straight line without torsion) a vector $\mathbf{r}(s)$ describing the position of the point of the centerline and a directors frame, $(\mathbf{d_1}(s), \mathbf{d_2}(s), \mathbf{d_3}(s))$ representing material directions. Under the above mentioned restrictions, the directors frame is a right-handed orthonormal basis and a member of the special orthogonal group SO(3) (the group of rotations of $\mathbb{R}^3$).

$$\begin{aligned} [0,L] &\to \mathbb{R}^3 \times \mathrm{SO}(3) \\ s &\mapsto (\mathbf{r}, (\mathbf{d_1}, \mathbf{d_2}, \mathbf{d_3})) \end{aligned}$$

The basis of directors is adapted to the curve: the third director $\mathbf{d}_3$ points in the tangent direction of the curve. The vectors $\mathbf{d}_1$ and $\mathbf{d}_2$ show the position of two material lines in the cross section of the rod. The evolution of the basis $(\mathbf{d}_k)_{1\leq k\leq 3}$ along the curve is represented by the Darboux vector ω. Similar to the angular velocity vector (replacing the time derivative with a derivative along the arc length), this vector has the following property:

$$\frac{\mathrm{d}\mathbf{d}_k}{\mathrm{d}s} = \omega \times \mathbf{d}_k \text{ for } k = 1,2,3$$

where × represents the cross-product.

2.2 Forces and torques

At the point of arc length s_0, the rod has a tension $\mathbf{n}(s_0)$ and an inner torque $\mathbf{m}(s_0)$. The rod is also submitted to external distributed forces like the weight or the contact forces, with a linear density f. The static equilibrium leads to

$$\begin{cases} \mathbf{0} = \frac{\mathrm{d}\mathbf{n}}{\mathrm{d}s}(s_0) \ + \mathbf{f}(s_0) \\ \mathbf{0} = \frac{\mathrm{d}\mathbf{m}}{\mathrm{d}s}(s_0) \ + \frac{\mathrm{d}\mathbf{r}}{\mathrm{d}s}(s_0) \times \mathbf{n}(s_0) \end{cases}$$

2.3 Material properties

We know from continuum mechanics that the torque at a point of a rod submitted to bending and torsion (See Figures 1 and 2) is

$$\mathbf{m}(s) = B_\tau \tau\, \mathbf{T} + B_\kappa \kappa\, \mathbf{B}$$

with κ the curvature, τ the torsion, $\mathbf{T} = \mathbf{d_3}$ the tangent and $\mathbf{B}$ the binormal. The coefficients B_κ and B_τ are defined in a similar way to the moments of inertia and depend on the material properties (Young's modulus E and shear modulus G) and the geometry of the cross section (See Figure 3. For a circular and homogeneous cross section with radius R, we have

- bending stiffness:

$$B_\kappa = EI = \iint_{crosssection} E x^2 \, dA = E\frac{\pi R^4}{4}$$

- torsional stiffness:

$$B_\tau = GJ = \iint_{crosssection} G r^2 \, dA = G\frac{\pi R^4}{2}$$

where x and r are the distances to the bending axis (in the cross-section, passing by the centerline) and to the torsion axis (the tangent to the centerline), respectively. In the case of a non-homogeneous cross section, the stiffnesses can be calculated by considering E and G as a function of the positions. In particular, for a hollow body like a hose, the result can be expressed with the help of the inner radius R_{inner}: $B_\kappa = E\frac{\pi(R^4 - R_{inner}^4)}{4}$

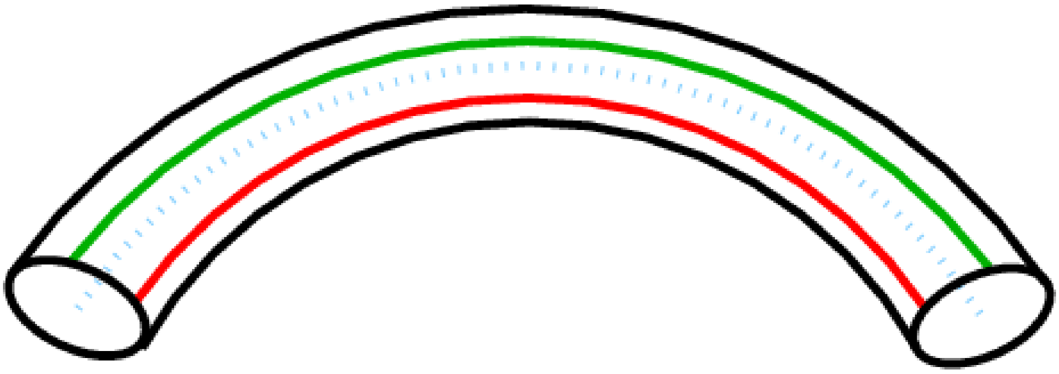

Fig. 1. Bending of a cable. The red, green and blue lines represent the trajectory of the endpoints of the three directors.

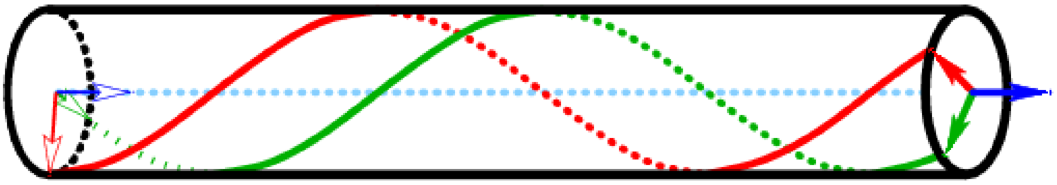

Fig. 2. Torsion of a cable.

2.4 Equations

The combination of these equations results in the following differential equations:

$$\begin{cases} \frac{\mathrm{d}\mathbf{n}}{\mathrm{d}s} &= -\mathbf{f} \\ \frac{\mathrm{d}\mathbf{m}}{\mathrm{d}s} &= -\mathbf{d}_3 \times \mathbf{n} \\ \frac{\mathrm{d}\mathbf{d}_k}{\mathrm{d}s} &= \omega \times \mathbf{d}_k \\ \omega &= \kappa_1 \mathbf{d}_1 + \kappa_2 \mathbf{d}_2 + \tau \mathbf{d}_3 \\ \mathbf{m} &= B_\kappa(\kappa_1 \mathbf{d}_1 + \kappa_2 \mathbf{d}_2) + B_\tau \tau \mathbf{d}_3 \end{cases}$$

These equations have the remarkable property that the torsion is constant over the length of the rod.

$$\tau = \tau_0$$

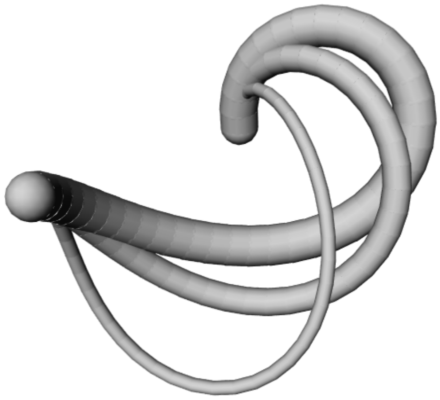

Fig. 3. Influence of the radius: the different radii lead to different stiffnesses B_κ and B_τ. The influence on the form of the cable can be important. A change in material parameters would also produce similar results.

2.5 Relation with the Frenet frame

Let us consider the Frenet frame (tangent **T**, normal vector **N** and binormal vector **B**) of the centerline. At any given point of the curve, the directors and the Frenet frames have at least a common vector, the tangent ($\mathbf{d}_3 = \mathbf{T}$). Therefore there is a rotation around $\mathbf{d}_3$ by an angle θ which transforms $(\mathbf{N},\mathbf{B},\mathbf{T})$ to $(\mathbf{d}_1,\mathbf{d}_2,\mathbf{d}_3)$. This angle θ shows the position of the material lines relatively to the Frenet frames: it is a “pure material torsion”. The Cosserat torsion is then the Frenet torsion τ_f (geometrical torsion of the centerline) augmented with this material torsion.

$$\tau = \tau_f + \frac{\mathrm{d}\theta}{\mathrm{d}s}$$

The Darboux vector is given by the following expression:

$$\omega = \kappa_1\,\mathbf{d}_1 + \kappa_2\,\mathbf{d}_2 + \tau\,\mathbf{d}_3$$

where κ_1 and κ_2 are the components of the curvature on $\mathbf{d}_1$ and $\mathbf{d}_2$:

$$\kappa\mathbf{B} = \kappa_1\,\mathbf{d}_1 + \kappa_2\,\mathbf{d}_2$$

3 First attempts

3.1 Shooting method for ODE

The Cosserat model gives us a set of ordinary differential equations where the tensions and inner moments are coupled to the positions and orientations. In order to solve this, we need to know either the forces, moments, position and orientation at one end of the cable, or a combination of them distributed over the two ends. Since it is much easier for the user in the absence of force feedback to specify the position and orientation at one point, for example with a spacemouse, we wanted to have boundary conditions of geometrical type (position and orientation) at both ends of the cable. We therefore have to solve the following problem: knowing the positions and the directors frames at the two endpoints, we are looking for the deformation of the cable under the condition that the length of the cable should remain constant. This is a so-called two-points-boundary-value problem where the boundary conditions are spread on the two endpoints of the integration interval.

The solution of Pai [8] is implemented for geometrical boundary conditions at one end of the strand and for dynamical boundary conditions at the other end, corresponding to the use of a haptic device. This particular configuration allows to solve the problem with two passes: the first one to calculate the forces and torques, and the second one in the opposite direction for the geometrical variables.

Unfortunately, an attempt to adapt this method to the desired type of boundary conditions was not successful. The usual method for solving such problems are so-called "shooting methods"[21]: there are two known and incomplete sets of boundary conditions, one at $s = 0$ and the other one at $s = L$. The method completes the set at $s = 0$, integrates the differential equation with these initial conditions, and considering the obtained final conditions as a function of the initial ones, looks iteratively (for example with a Newton algorithm) for the appropriate initial conditions. Unfortunately, the initial conditions are difficult to determine, and the search does not always converge and sometimes aborts, for example when the curvature radius at a point is of the same order of magnitude as the integration step length. Furthermore, such an approach makes it difficult to integrate external forces such as contact forces.

3.2 Simple spring-mass-model

In order to avoid these difficulties, we experimented with a different approach using a spring-mass system. The rod is modeled as a sequence of mass points (lying on the centerline of the cable) which are connected with different kinds of springs: linear springs for the length conservation and torsion springs for the bending. The knowledge of the centerline leaves one degree of freedom unspecified, namely the material rotation around the centerline.

Since the Cosserat theory also considers the material direction, we use a new variable, θ, at each point to represent the angle between the Frenet and the directors frames (See 2.5). The global torsion is the sum of both the Frenet torsion - calculated from the coordinates of the mass points - and the pure material torsion - calculated as the derivative of the fourth coordinate θ-. The energy is then $E = \frac{1}{2}(B_\kappa \kappa^2 + B_\tau \tau^2)$ and the forces are calculated as the negative of the gradient of the energy.

We studied two ways of computing the Frenet torsion: one using the binormal vector and one using a function of the derivatives of the coordinates. For the first one, since $\mathbf{B}$ is a unit vector, the change of $\mathbf{B}$ is a rotation and the torsion is - in the discretized system - proportional to the angle between the two binormal vectors at the points i and $i+1$:

$$\tau_f = \frac{\angle(\mathbf{B}_i, \mathbf{B}_{i+1})}{|s_{i+1} - s_i|}$$

where s_i is the arc length at point i. Since the plane defined by the three points $i-1$, i, $i+1$ contains the tangent $\mathbf{T}$ and the normal $\mathbf{N}$, the binormal at point i is orthogonal to both $\mathbf{u_{i-1}}$ and $\mathbf{u_i}$ and is calculated as:

$$\mathbf{B}_i = \frac{\mathbf{u_{i-1}} \times \mathbf{u_i}}{||\mathbf{u_{i-1}} \times \mathbf{u_i}||}$$

with $\mathbf{u_i}$ the unit vector between $\mathbf{r}(s_i)$ and $\mathbf{r}(s_{i+1})$:

$$\mathbf{u_i} = \frac{\mathbf{r}(s_{i+1}) - \mathbf{r}(s_i)}{||\mathbf{r}(s_{i+1}) - \mathbf{r}(s_i)||}$$

This scheme has two problems: it is extremely sensitive to noise in the position of the mass points where the curvature is small, and it does not have well-defined binormals at inflexion points. As an example of the first, suppose that vectors $\mathbf{u_{i-1}}$ and $\mathbf{u_i}$ are fixed, and the angle between $\mathbf{u_i}$ and $\mathbf{u_{i+1}}$ is small, a very small change in $\mathbf{u_{i+1}}$ could mean a huge difference for τ_f, just like at the Earth poles a small change in position can mean a large change in longitude. Accordingly, the forces in case of a small curvature are huge, which leads to numerical instability and impedes the convergence.

For the second, the binormals are not defined at such points and undergo a discontinuity (opposite directions). In a configuration with (almost) inflexion points, the direction of the binormal can change sign from one iteration to the next, which of course is impractical. An easy solution is to precalculate the binormal before each iteration and, when necessary, to multiply it by -1 in order to ensure $\mathbf{B}_i^T \mathbf{B}_{i+1} \geq 0$, and to keep these places in memory to take into account the possible sign changes for the subsequent calculations.

Curvature and torsion could instead be calculated as functions of the derivatives of $\mathbf{r}(s)$. After discretization and simplification, the expressions for the curvature and the torsion become

$$\kappa = \frac{1}{2L} \|\mathbf{u_i} \times (\mathbf{u_{i+1}} - \mathbf{u_{i-1}})\|$$

$$\tau_f = \frac{1}{L^3\kappa^2} \mathbf{u_i}^T (\mathbf{u_{i+1}} \times \mathbf{u_{i-1}})$$

with L the length of a segment. This scheme is more stable and less noise-sensitive as the previous one, but it is still insufficient. The torsion remains in both cases the problem. Consequently, another way of calculating the torsion is needed.

4 Implementation

4.1 Mixed coordinates

We are looking for a coordinate system in which the torsion is easily expressed and not too noise-sensitive. The torsion depends on the difference of orientation along the tangent to the centerline of two segments. This orientation can be described as a rotation of $SO(3)$ from a reference orientation. From the several representations of rotations of $SO(3)$, we have chosen unit quaternions. (Quaternions are 4-tuples that can be seen as a generalization of complex numbers. They will be described in more detail in section 5) Many properties speak in favor of unit quaternions: they only have 4 coordinates and one constraint (they must have a unit length), which is an advantage compared to rotation matrices (with 9 components and 6 constraints). Furthermore, the rotation of a vector is easily expressed and the composition of two rotations can also be easily calculated as the product of the two corresponding quaternions. This group structure is an advantage for the simulation. Quaternions also lack singular points and gimbal lock, contrarily to Euler or Cardan angles. So we use a system with seven coordinates for each point: the three usual space coordinates and a quaternion which represents the orientation of a segment between two points (See Figure 4)

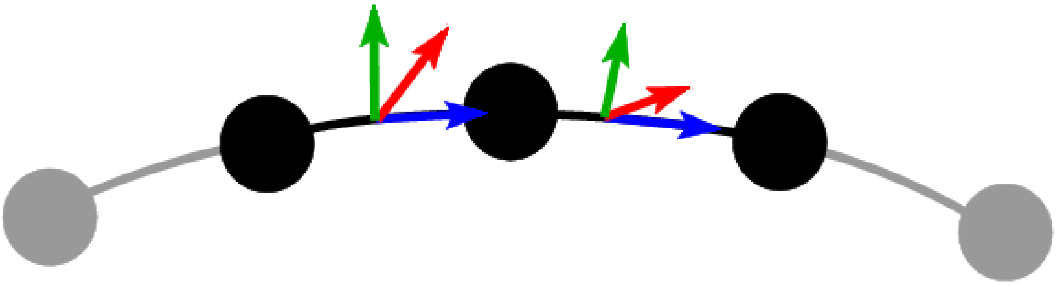

Fig. 4. Discretization of a cable: the black points have three spatial coordinates. Between two points, a quaternion represents the orientation of the director frame.

4.2 Notation

The following notations will be used in the rest of the paper:

n is the number of discretization points of the cable. The cable begins and ends with a discretization point and the centerline is linearly interpolated between two points. $\mathbf{X} \in \mathbb{R}^{7n-4}$ is the vector of all coordinates of the cable and therefore of all scalar unknowns. $X_i \in \mathbb{R}$ is the i-th component of $\mathbf{X}$. $\mathbf{x_i} \in \mathbb{R}^3 = (X_{7i+1}, X_{7i+2}, X_{7i+3})$ is the position of the point i (for $1 \leq i \leq n$). $\mathfrak{q}_i \in \mathbb{R}^4 = (X_{7i+4}, X_{7i+5}, X_{7i+6}, X_{7i+7})$ is a quaternion representing the orientation of the segment between the points i and $i+1$ (for $1 \leq i \leq n-1$).

As far as the orientations are concerned, we can arbitrarily choose a right-handed orthonormal basis of $\mathbb{R}^3$ as an orientation reference. The orientation of the segment i is then the image of the rotation represented by the quaternion $\mathfrak{q}_i$ of the reference orientation - in our case a basis whose third vector is in the direction $\mathbf{ref} = (0,1,0)$. This choice corresponds to the default orientation of the axis of a cylinder in OpenInventor/OpenGL, which will simplify the graphical representation afterwards since the quaternion can be used to directly specify the rotation of the cylinder representing the segment.

Additionally, $E \in \mathbb{R}$ is the energy. $\mathbf{F} \in \mathbb{R}^{7n-4}$ is the vector of all forces; $F_i \in \mathbb{R}$ is the i-th component of $\mathbf{F}$. $\mathbf{H} \in \mathbb{R}^{7n-4 \times 7n-4}$ is the Hessian: $H_{i,j} = \frac{\partial^2 E}{\partial X_i \partial X_j}$.

L_{ref} is the reference length for each segment. It is equal to the total length of the cable divided by the number of segments $(n-1)$. $L_i = \sqrt{(\mathbf{x_{i+1}} - \mathbf{x_i})^2}$ is the actual length of segment i.

5 Forces

The interactions taken into account are bending and torsion, weight, stretch (inextensibility), normalization of quaternions and coherence between the quaternions and the space coordinates. Handles (fixed points) can be defined optionally: each one defines the additional constraint that the cable should pass by a particular point with a particular orientation. By default, the two endpoints are considered to be fixed in position and orientation: their coordinates are excluded from the solver range.

The use of space coordinates and quaternions allows to apply the forces to the most appropriate kind of coordinates (see Table 1).

The main disadvantage of this method is the increased number of variables ($7n-4$ instead of $4n$). But since every type of interaction is relatively easy to calculate and since the Hessian is strongly banded (each interaction can be expressed as a sum

	Positions only	Orientations only	Positions and orientations
Model internal	length conservation	quaternion norm	coherence
Model external	weight	bending and torsion	-

Table 1
Summary of the different interactions

over neighboring vertexes or segments), the system as a whole is easy to solve (see section 6)

5.1 Derivation of the forces

For each kind of interaction, we first define an energy function and then derive the forces from this function, following the use in mechanics:

$$F_i = -\frac{\partial E}{\partial X_i}$$

We also define the symmetric Hessian matrix $\mathbf{H} \in \mathbb{R}^{7n-4\times 7n-4}$, such that

$$H_{i,j} = \frac{\partial^2 E}{\partial X_i \partial X_j} = -\frac{\partial F_i}{\partial X_j}$$

Since each type of interaction can be decomposed as a sum of interactions between either two points, two quaternions or two points and a quaternion, we calculate the energy, the forces and the Hessian as a sum over these element groups. In order to enhance the calculation speed, it is important to calculate only once the partial terms that appear several times in the three functions.

For a global position $\mathbf{X}$, we can formulate the energy as the sum of the energies over all points and segments and over all interactions.

$$\begin{aligned}
E = & \sum_{Interactions} \sum_i E_{Interaction,i} \\
= & \sum_{i=1}^{n-1} E_{Length,i} + \sum_{i=1}^{n-1} E_{QuatNorm,i} \\
& + \sum_{i=1}^{n} E_{Weight,i} + \sum_{i=1}^{n-1} E_{Coh,i} \\
& + \sum_{i=1}^{n-2} E_{Bending,i} + \sum_{i=1}^{n-2} E_{Torsion,i}
\end{aligned}$$

The forces and the Hessian can be calculated in a similar way. In the following, $k_{Interaction}$ is the constant relative to the interaction $Interaction$ that will be used for defining the relative weights of the different interactions in the energy function.

5.2 Stretch forces and conservation of the length

In practice, cables are unstretchable: the length of each segment has to be kept constant. For this purpose we use strong linear springs for which the energy is defined classically as

$$E_{Length,\,i} = \frac{1}{2}k_{Length}(L_i - L_{ref})^2$$

where k_{Length} is the constant of the spring. The force on the point $\mathbf{x}_i$, just opposed to the force on point $\mathbf{x}_{i+1}$, is

$$\mathbf{F}_{Length,i} = k_{Length}\mathbf{u}_i(L_i - L_{ref})$$

If we consider only this spring, the minimum of the energy is clearly at $L_i = L_{ref}$. But the points i and $i+1$ are also submitted to other interactions that result in a disturbing force that stretches (or compresses) the spring. Since the spring can only exert a force when it is not at equilibrium, it alone cannot enforce exactly the constraint of a constant length: we use an additional force to achieve this. If we look at control theory, a spring alone is a proportional controller: the actuating variable (the force) is proportional (with the proportionality constant k_{Length}) to the difference between the desired value (L_{ref}) and the actual one (L_i). The forces for segment i between point i and $i+1$ due to the stretch forces are

$$\mathbf{f}_{P,\,i} = -\mathbf{f}_{P,i+1} = k_{Length}(L_i - L_{ref})\mathbf{u_i}$$

We want to use the equivalent of a PI-(proportional-integral) controller, which has the property of being able to enforce a constraint exactly so that the steady-state error is null. The PI-controller combines a proportional part (the spring) with an integral one. Its actuating variable is proportional to the integral over the time of the difference between the desired and actual values. When the error is null, the proportional force is also null, but the integral one counteracts the perturbations. The proportional force is nonetheless essential to the stability of the system. As a consequence of the presence of the integral force, the proportional constant can be reduced (in comparison with a spring-only system), which makes the system less stiff as a whole. To implement this, we add constant forces $f_{I,\,i}\mathbf{u_i}$ on point i and $-f_{I,\,i}\mathbf{u_i}$ on point $i+1$. This force must have the same direction as the proportional one. The total force on point i due to the stretch of segment i is then

$$\mathbf{f}_i = (f_{I,\,i} + k_{Length}(L_i - L_{ref}))\mathbf{u_i}$$

This corresponds to an energy of

$$E_{Length,\, i} = \frac{1}{2} k_{Length} (L_i - L_{ref})^2 + f_{I,\, i} (L_i - L_{ref})$$

We have now $n-1$ additional parameters $f_{I,\, i}$. For solving the system, we use an iterative approach: we first solve the system holding the $f_{I,\, i}$ constant, then adjust their values in function of the result and solve anew the system until an equilibrium is reached (The constraints are enforced within an ε tolerance that should be chosen slightly bigger than the numerical precision of the system solver).

For updating the integral forces, we adjust each one individually: the new force is the old one augmented with the difference of lengths multiplied by a constant

$$f_{I,\, i,\, new} = f_{I,\, i,\, old} + k_{I,\, Length} (L_i - L_{ref})$$

This constant $k_{I,\, Length}$should not have a value too big compared to k_{Length} for ensuring stability.

5.3 Weight

The weight has an important influence on the form of sagging cables since it determines the direction of the deformation of the cable. The longer the cable is and the smaller the ratio of the distance between the two end points and the length of the cable is, the greater is the influence of the weight. Furthermore, in particular undetermined cases (like a cable in which the two end tangents are collinear with the line joining the two end points) where there would be an infinite number of solutions without gravity, it allows to eliminate the ambiguity.

We consider the cable as a chain of mass points with equal masses m. The total mass of the cable is $n\, m$. The energy is $E_{Weight,i} = -m\mathbf{g}^T\mathbf{x_i}$ where $\mathbf{g} \in \mathbb{R}^3$ is the acceleration of gravity. The force is then $\mathbf{F}_{Weight,i} = m\mathbf{g}$. Since the force does not depend on any of the coordinates, the weight has no contribution to the Hessian.

5.4 Coherence between quaternions and positions

For the correct functioning of the model, it is important to ensure that the quaternions (and thus the bending and torsion forces and torques) are correctly coupled to the positions. The unit vector $\mathbf{u}_i = \frac{\mathbf{x}_{i+1} - \mathbf{x}_i}{||\mathbf{x}_{i+1} - \mathbf{x}_i||} \in \mathbb{R}^3$ in the direction between the two points i and $i+1$ should be equal to the reference direction **ref** rotated by the quaternion $\mathfrak{q}_i$.

Let us consider a rotation of an angle θ around an axis $\mathbf{v} \in \mathbb{R}^3$ (with $||\mathbf{v}|| = 1$). The corresponding quaternion is then

$$\mathfrak{q} = (q_0, q_1, q_2, q_3) = (q_0, \mathbf{q}) = \left(\cos\frac{\theta}{2}, \sin\frac{\theta}{2}\mathbf{v}\right)$$

The image $\mathbf{b} \in \mathbb{R}^3$ of a vector $\mathbf{a} \in \mathbb{R}^3$ by a rotation represented by a quaternion $\mathfrak{q}$ can be calculated by: $(0, \mathbf{b}) = \mathfrak{q} \cdot (0, \mathbf{a}) \cdot \overline{\mathfrak{q}}$ where $\overline{\mathfrak{q}} = (q_0, -\mathbf{q})$ is the conjugated of $\mathfrak{q}$ and where the quaternion product

$$\mathfrak{p} \cdot \mathfrak{q} = (p_0 q_0 - \mathbf{p}^T \mathbf{q}, p_0 \mathbf{q} + q_0 \mathbf{p} + \mathbf{p} \times \mathbf{q})$$

is used. For a constant $\mathbf{ref} = (0, 1, 0)$, the image can be directly calculated as

$$Rot(\mathbf{ref}) = (2(q_1 q_2 - q_0 q_3), q_0^2 - q_1^2 + q_2^2 - q_3^2, 2(q_0 q_1 + q_2 q_3).$$

The energy is defined as

$$E_{Coh,i} = \frac{1}{2} k_{Coh} ||(0, \mathbf{u_i}) - \mathfrak{q}_\mathbf{i} \cdot (0, \mathbf{ref}) \cdot \overline{\mathfrak{q}_\mathbf{i}}||^2$$

In the same manner as for the length conservation, we introduce an integral force for each of the three components of the coherence between quaternions and positions.

5.5 Quaternion norm

Since quaternions represent a pure rotation only when they have a unit norm - otherwise a scaling effect is introduced and a very small curvature and torsion could be obtained- , the norm of the quaternions must be maintained unitary. The energy is simply defined as

$$E_{QuatNorm,i} = \frac{1}{2} k_{QuatNorm} \left(||\mathfrak{q}_\mathrm{i}|| - 1 \right)^2$$

for $i \in 1...n-1$ with $||\mathfrak{q}|| = \sqrt{q_0^2 + q_1^2 + q_2^2 + q_3^2}$. This term only depends on the quaternion $\mathfrak{q}_i$.

This term is normally easy to enforce and does not pose any difficulty. However, in the case of a cable with very high bending and torsion constants, it can happen that the cable takes a ”V” shape with a very sharp bend: the norm of a particular (or two) quaternion(s) collapse to almost 0. The interactions affected by the norm of a quaternion are the bending and torsion (κ and τ are proportional to the norm of ω and consequently to the norm of each of the concerned quaternions, see section 5.6) and the coherence (the norm of the ”rotation” of the reference direction is proportional to the square of the norm of the quaternion, see section 5.4). Whereas the coherence term is limited (the norm of the vector $\mathbf{u}_i - Rot(\mathbf{ref})$ cannot be greater than 2 in general and practically than 1 in this particular case), all the actual bending of the cable is absorbed by this particular point and the global bending and torsion energy tend to 0.

The solution is then to change the formulation of the energy as a function of the inverse of the norm:

$$E_{QuatNorm,i} = \frac{1}{2} k_{QuatNorm} \left(\frac{1}{\|\mathfrak{q}_\mathfrak{i}\|} - 1 \right)^2$$

If the norm tends to 0, the energy will then tend to the infinite, thus canceling all global energy diminution.

If desired, this definition could be taken for the norm smaller than 1 and the old one for the norm greater than one. The resulting function is $\mathscr{C}^2$ (the function and its first two derivatives are continuous in all points and in particular where $\|\mathfrak{q}_\mathfrak{i}\| = 1$), which means that there are no problems for the numerical resolution and that the behavior of the system should not change significantly near the equilibrium point $\|\mathfrak{q}\| = 1$. However this may not be necessary since a norm greater than 1 augments both the coherence and the bending and torsion energy.

5.6 Bending and torsion

The bending and torsion forces are calculated jointly as a function of the relative rotation between two segments. (See Figure 5 for effects of the torsion.) They are determined by the two consecutive quaternions $\mathfrak{q}_i$ and $\mathfrak{q}_{i+1}$. (Observe that the previous formulations needed three segments and that the Frenet torsion is not needed anymore.) The relative rotation from segment i to segment $i+1$ is represented by

$$\mathfrak{q}_{i \to i+1} = \mathfrak{q}_{i+1} \overline{\mathfrak{q}_i}.$$

(The inverse of a quaternion $\mathfrak{q}$ is $\frac{\overline{\mathfrak{q}}}{\|\mathfrak{q}\|}$ and for unitary quaternions simply $\overline{\mathfrak{q}}$.).

The Darboux vector is, in global coordinates, for a differentiable function $\mathfrak{q}(s)$ and where the dot represents the derivation with respect to the arclength s: $\dot{\mathfrak{q}} = \frac{\partial \mathfrak{q}}{\partial s}$,

$$(0, \boldsymbol{\omega_g}) = 2\dot{\mathfrak{q}} \cdot \overline{\mathfrak{q}}$$

and in local coordinates

$$(0, \boldsymbol{\omega_l}) = 2\overline{\mathfrak{q}} \cdot \dot{\mathfrak{q}}$$

They can be discretized as

$$\boldsymbol{\omega_g} = \frac{2}{L} \overrightarrow{\mathfrak{q}_{i+1} \cdot \overline{\mathfrak{q}}_i}$$

and

$$\boldsymbol{\omega_l} = \frac{2}{L} \overrightarrow{\overline{\mathfrak{q}}_i \cdot \mathfrak{q}_{i+1}}$$

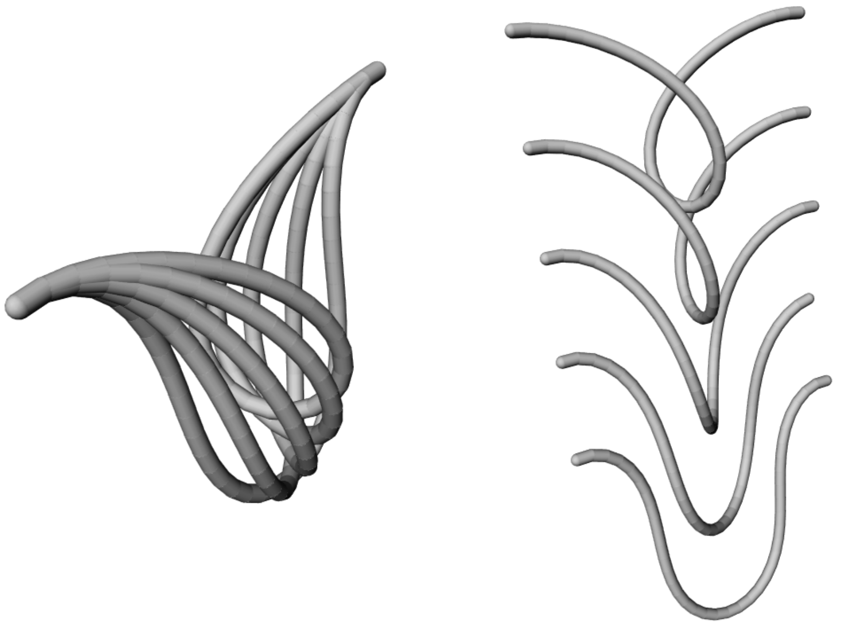

Fig. 5. Influence of the torsion: the same cable is submitted to different values of the torsion by rotating one of its extremities

On the other hand, the general properties of the Darboux vector give

$$\omega = \kappa \mathbf{B} + \tau \mathbf{T}.$$

We can now calculate the curvature and the torsion: a decomposition of ω on the basis formed by $\mathbf{T}$ and $\mathbf{B}$ (which is defined as the direction of the residual component $\omega - \tau \mathbf{T} = \kappa \mathbf{B}$) gives us:

$$\tau = \omega^T \mathbf{T}$$

and

$$\kappa = \|\omega - \tau \mathbf{T}\| .$$

Considering the expression in the local base leads to simplifications: **T** is the image of the rotation of the reference direction **ref**. The local base is also the image of the same rotation of the canonical base of $\mathbb{R}^3$. Hence **T** is the direction **ref** in the local base.

$$\tau = \omega^T \mathbf{T} = \omega_l^T \mathbf{ref}$$

In the particular case of $\mathbf{ref} = (0, 1, 0)$,

$$\omega_l = (\kappa_1, \tau, \kappa_2)$$

where $\kappa^2 = \kappa_1^2 + \kappa_2^2$. Coupled with the discretization $\boldsymbol{\omega_l} = \frac{2}{L}\overrightarrow{\overline{\mathrm{q}}_i \cdot \mathrm{q}_{i+1}}$, we now have an easy way to calculate the bending and torsion energy:

$$E_{BendingTorsion,i} = E_{Bending,i} + E_{torsion,i} = \frac{1}{2} B_\kappa \kappa^2 + \frac{1}{2} B_\tau \tau^2$$

which can be rewritten as

$$\begin{aligned} E_{BendingTorsion,i} &= \tfrac{1}{2} (B_\kappa \omega^T \omega + (B_\tau - B_\kappa)(\omega^T \mathbf{T})^2) \\ &= \tfrac{1}{2} \omega^T (B_\kappa \mathbf{I}_3 + (B_\tau - B_\kappa)\mathbf{T}\mathbf{T}^T) \omega \end{aligned}$$

The matrix $(B_\kappa \mathbf{I}_3 + (B_\tau - B_\kappa)\mathbf{T}\mathbf{T}^T)$ has the eigenvalues B_τ (for vectors collinear with $\mathbf{T}$) and B_κ (for vectors orthogonal to $\mathbf{T}$) which shows that the bending and torsion energy is nothing else than the square of a particular (local) norm of ω as long as the two constants are positive.

A possibility would be to use only the quaternions as coordinates and calculate iteratively the positions. The length conservation and coherence forces would then disappear. The disadvantage is that the system matrix would be a full matrix (the position of point i depends on all the quaternions between 1 and $i-1$), which makes the calculation much slower. External forces like contact forces would also be difficult to implement.

In the case where the rest state has a non-zero curvature or torsion (which is the case, for example, for molded hoses), the energy becomes

$$E_{BendingTorsion,i} = \frac{1}{2} B_\kappa (\kappa_1 - \kappa_{1,0})^2 + \frac{1}{2} B_\kappa (\kappa_2 - \kappa_{2,0})^2 + \frac{1}{2} B_\tau (\tau - \tau_0)^2$$

where $\kappa_{1,0}$, $\kappa_{2,0}$, τ_0 are the values of the components of the curvature and of the torsion in the rest state (See Figure 6) . The form of the cable can be greatly influenced by this rest state deformation. Some hoses also show a rest curvature due for example to a storage on a roll. It is a cause for the variability between hoses.

For cables which do not have a circular cross-section or whose material repartition is not symmetric, we can simply take the energy to be of the form

$$E_{BendingTorsion,i} = \frac{1}{2} B_{\kappa 1} \kappa_1^2 + \frac{1}{2} B_{\kappa 2} \kappa_2^2 + \frac{1}{2} B_\tau \tau^2$$

where $B_{\kappa 1}$ and $B_{\kappa 2}$ are the bending constants around the two axes corresponding to the two directors $\mathbf{d}_1$ and $\mathbf{d}_2$ (assuming that they are principal axes).

5.7 Handles

Each handle (fixed point) is attached either to a point or to a segment. The two possibilities are offered for an easy interface with the graphical representation: the user can attach it either to a sphere or a cylinder. The handle can fix either only the

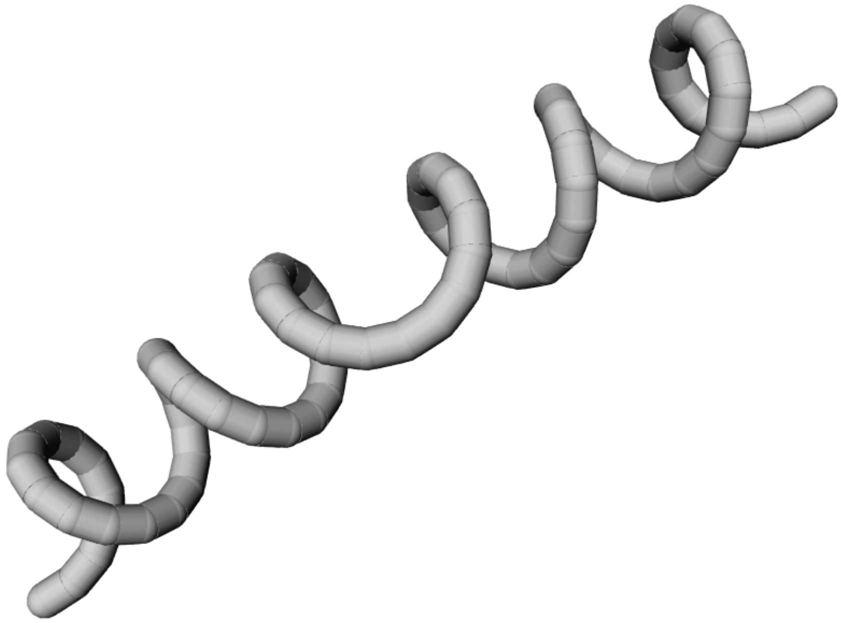

Fig. 6. Effect of a rest curvature on the form of the cable: the cable shows a characteristic ”phone cable”-look

position or both the position and orientation at a point. In the case of a sphere, the orientation is taken as the (normed) mean value of the two quaternions surrounding it; in the case of a cylinder, the position is the mean value of the positions of the two surrounding points. If a handle is associated with the point $\mathbf{x_i}$ and with the quaternion $\mathfrak{q}_\mathbf{i}$, the energy is

$$E_{HandleSphere,i} = k_{Handle}((\mathbf{x}_i - \mathbf{x}_{Handle})^2 + (\frac{\mathfrak{q}_{i-1} + \mathfrak{q}_i}{\|\mathfrak{q}_{i-1} + \mathfrak{q}_i\|} - \mathfrak{q}_{Handle})^2)$$

or

$$E_{HandleCylinder,i} = k_{Handle}(\frac{\mathbf{x_i} + \mathbf{x_{i+1}}}{2} - \mathbf{x}_{Handle})^2 + (\mathfrak{q}_i - \mathfrak{q}_{Handle})^2)$$

Handles on spheres tend to have the problem that they “bend”, especially with low bending constants: the mean value of the two quaternions at this point is conformed with the desired value for the handles, but the two quaternions may have very different values, leading to a sharp bend in the cable. To remedy this problem, we replace the energy by

$$E_{HandleSphere,i} = k_{Handle}((\mathbf{x}_i - \mathbf{x}_{Handle})^2 + (\frac{\mathfrak{q}_{i-1} + \mathfrak{q}_i}{2} - \mathfrak{q}_{Handle})^2)$$

Due to the absence of normalization, the norm of the “mean quaternion” is, assuming that both quaternions $\mathfrak{q}_{i-1}$ and $\mathfrak{q}_i$ have a unit norm,

$$\left\| \frac{\mathfrak{q}_{i-1} + \mathfrak{q}_i}{2} \right\| = \cos \frac{\theta}{2}$$

where θ is both the angle between the two quaternions in quaternion space and the angle of the relative rotation between them as the following calculation shows:

$$\mathfrak{q}_{i-1}^T \mathfrak{q}_i = q_{i-1,0} q_{i,0} + \mathbf{q}_{i-1}^T \mathbf{q}_i = (\mathfrak{q}_i \cdot \overline{\mathfrak{q}}_{i-1})_0$$

The norm of the difference $\frac{\mathfrak{q}_{i-1}+\mathfrak{q}_i}{2} - \mathfrak{q}_{Handle}$ is then at minimum $1 - \cos \frac{\theta}{2}$. In the case of a sharp bend, this term augments the energy and counteracts the effect.

5.8 Contact forces

When a collision is detected (the mass point i has penetrated into another body), we apply a spring and an integral force at this point to keep it on the surface. Let $\mathbf{y} \in \mathbb{R}^3$ be the orthogonal projection of $\mathbf{x_i}$ on the surface and $\mathbf{n} \in \mathbb{R}^3$ the normal at $\mathbf{y}$, oriented towards the outside and normed. The penetration distance is then $d = (\mathbf{y} - \mathbf{x_i})^T \mathbf{n}$ (d is positive when $\mathbf{x}$ is inside of the body) and the force is

$$\mathbf{f_{Collision,\, i}} = k_{Collision}\, d\mathbf{n} + f_{I,\, Collision,\, i}\mathbf{n}$$

and the energy

$$E_{Collision,\, i} = \frac{1}{2} k_{Collision}\, d^2 + f_{I,\, Collision,\, i}\, d$$

When the penetration distance of a point is 0 (within the tolerance) and its integral force $f_{I,\, Collision,\, i}$ is negative, it means that the point needs to be attracted towards the object in order to be on the surface: in this case, it is not a collision point anymore and the spring and the integral forces are removed. (See Figure 7)

$f_{I,Collision,i}$ can be updated with two different methods: an individual or a global one. The first method is similar to the one we used for the length:

$$f_{I,i,new} = f_{I,i,old} + k_{I,Collision} d$$

The second method uses the derivative of the forces as a predictor for the behavior of the system upon a small change of the values of the forces. The Taylor series for the forces (excluding the integral force) is $\mathbf{F}(\mathbf{X}+\mathbf{h}) = \mathbf{F}(\mathbf{X}) - \mathbf{H}\mathbf{h}$ with $\mathbf{h} \in \mathbb{R}^{7n-4}$ the difference between the old and the new position. Since both the old and the new position are equilibriums, we have $\mathbf{F}(\mathbf{X}) + f_{I,\, Collision,\, i}\tilde{\mathbf{n}} = \mathbf{0}$ and $\mathbf{F}(\mathbf{X}+\mathbf{h}) + (f_{I,\, Collision,\, i} + \Delta f_I)\tilde{\mathbf{n}} = 0$ with $\tilde{\mathbf{n}} \in \mathbb{R}^{7n-4}$ the ”direction” of the constraint: $\tilde{n}_k = 0$ except for the block corresponding to $\mathbf{x}_i$: ($\tilde{n}_{7i+1}$, $\tilde{n}_{7i+2}$, $\tilde{n}_{7i+3}$) that take the values

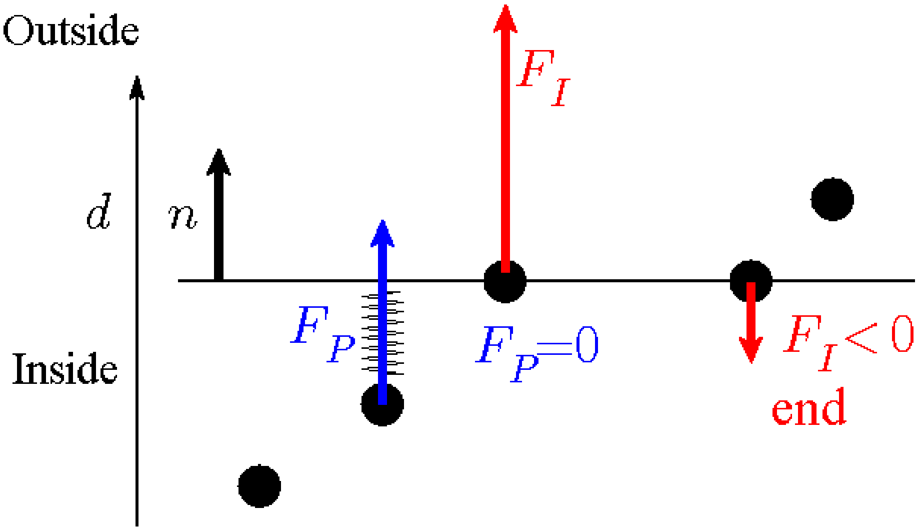

Fig. 7. Principle of the collision treatment: when the point is on the surface, the proportional force is 0, but the integral force maintain it in position. When the integral force is negative, the point is attracted artificially to the surface: the contact is broken.

of $\mathbf{n}$. Combining these three equations gives

$$\Delta f_I \tilde{\mathbf{n}} = \mathbf{H}\mathbf{h}$$

In order to fulfill the non-penetration constraint, we need that

$$\mathbf{h}^T \tilde{\mathbf{n}} = d$$

These two equations lead to

$$\Delta f_I = \frac{d}{\tilde{\mathbf{n}}^T \mathbf{H}^{-1} \tilde{\mathbf{n}}}$$

In the case of several contact points, the new force is such that

$$\mathbf{F}(\mathbf{X}+\mathbf{h}) + \sum_{i \in Contact points} \Delta f_{I,i} \tilde{\mathbf{n}}_{\mathbf{i}} = 0$$

and the conditions to fulfill $\tilde{\mathbf{n}}_{\mathbf{i}}^T \mathbf{h} = d_i$. The combination of these relations results in a matrix equation:

$$\mathbf{M}(\Delta f_{I,1}, ..., \Delta f_{I,c})^T = (d_1, ..., d_c)^T$$

with c the number of contact points and $\mathbf{M} \in \mathbb{R}^{c \times c}$ a matrix such that $\mathbf{M}_{i,j} = \tilde{\mathbf{n}}_{\mathbf{i}}^T \mathbf{H}^{-1} \tilde{\mathbf{n}}_{\mathbf{j}}$. Although we have to solve the above system, this method converges experimentally much faster than the other: it only needs one or two iterations to find the correct values for the f_I. It cannot be used as such in the case of the length conservation or of the coherence between positions and quaternions since the direction $\tilde{\mathbf{n}}$ would not be constant. (See Figure 8)

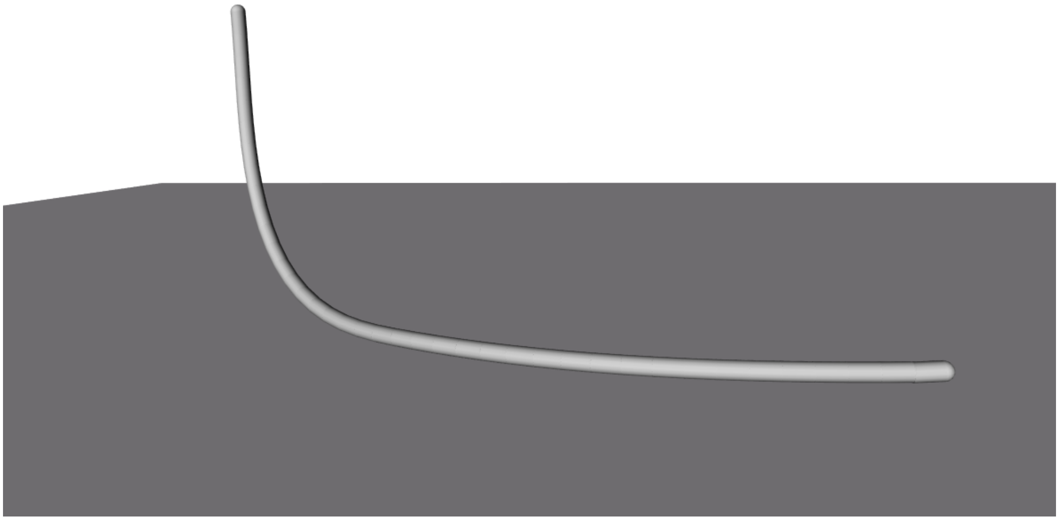

Fig. 8. Deformation of a cable due to the contact to a plane

6 Solver

6.1 General principles

Since the cables and hoses do not have a high dynamic range, considering a static solution at each time step is sufficient for most of the applications we are concerned with, like wire routing or assembly simulation. Dynamic phenomena like fast oscillations are excluded by the quasi-static system: the system is after each time step at equilibrium. Numerical oscillations, which are often a problem for stiff spring-mass systems, are also excluded by the absence of speeds as variables. We use an energy minimizing algorithm for solving the system. Note that the system could be easily modified to become a dynamic one, introducing the velocities as supplementary variables and solving the system, for example with the algorithm proposed by Baraff [11]. It would be necessary to add damping forces for each kind of interaction, following the formulation of Baraff: if the constraint is $C(\mathbf{X}) = 0$, the energy is $E = \frac{1}{2}kC(\mathbf{X})^T C(\mathbf{X})$, the forces are of the form $-k\frac{\partial C(\mathbf{X})}{\partial \mathbf{X}}C(\mathbf{X})$ and the damping forces of the form $-k\frac{\partial C(\mathbf{X})}{\partial \mathbf{X}}\dot{C}(\mathbf{X})$. All the interactions except the weight (for which there is no damping force physically speaking) can obviously be rewritten in this form.

If the norm of the forces vector $\mathbf{F}$ is null (in practice small enough $\|\mathbf{F}\| < \varepsilon$ in order to account for numerical error), the system is at equilibrium and we have the solution we were looking for. If not, we minimize the energy until we find an equilibrium. The basic hypothesis is that the new solution (for slightly modified conditions: a point has been moved between the two frames for example) should be near to the old one, and the old solution vector $\mathbf{X}_{old}$ can thus be used as a good starting point for the search of the new solution.

Our algorithm is iterative. In each loop, a sequence of different algorithms is used until a smaller value for the energy is found. If a particular algorithm gives a solution, $\mathbf{X}_{old}$ is replaced by the new solution and a new loop begins until the equilibrium is reached. If it does not find a better solution, the next algorithm is used. When the difference either in position $\|\mathbf{X}_{new} - \mathbf{X}_{old}\|$ or in energy $\|E_{new} - E_{old}\|$ is smaller than a predetermined value, the loop is stopped. The different algorithms that we use are in order: Newton's method applied to the forces, the non-linear conjugate gradient method, the linear conjugate gradient method, the steepest descent method and if all else fails, a line search along the forces. It is important to note that in the vast majority of the cases, only the first or the first two are used; the other algorithms serve as a security for particular stiff cases or for tuning the different constants for the interactions. This structure allows us to have at the same time a fast response in usual cases while retaining the robustness necessary to deal with stiff cases. Thanks to the formulation of the energies and this iterative, the mean calculation time for an iteration is practically a linear function of the number of discretization points. (See Figure 9)

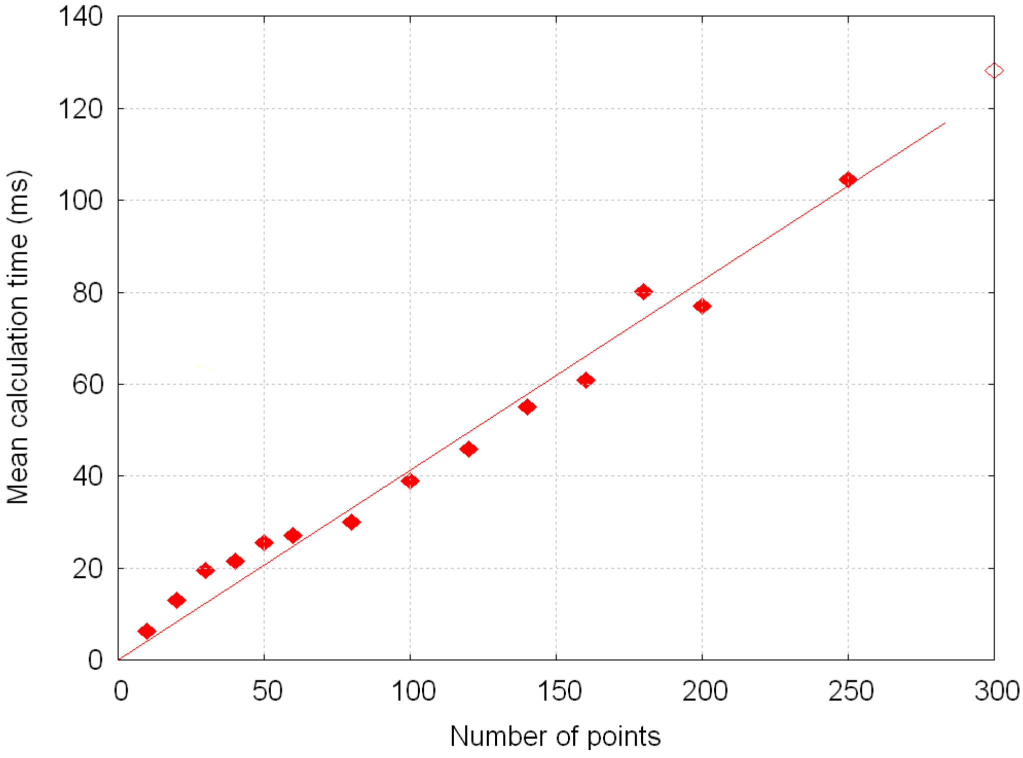

Fig. 9. Influence of the number of discretization points on the mean calculation time: the calculation tim is roughly a linear function of the number of points.

The first algorithm is the Newton Method applied to the forces. It is particularly efficient near the equilibrium. However, it is well-known that it only converges if the starting solution is near enough to the equilibrium. If the energy in a point $\mathbf{X}+\mathbf{h}$ is approximated by the Taylor series in $\mathbf{X}$, $E_{approx}(\mathbf{X}+\mathbf{h}) = E(\mathbf{X}) - \mathbf{F}^T\mathbf{h} + \frac{1}{2}\mathbf{h}^T\mathbf{H}\mathbf{h}$. This approximation finds its minimum when its gradient is null, i.e. for $-\mathbf{F}+\mathbf{H}\mathbf{h} = 0$ which leads to $\mathbf{h} = \mathbf{H}^{-1}\mathbf{F}$ and $\mathbf{X_{new}} = \mathbf{X_{old}} + \mathbf{H}^{-1}\mathbf{F}$. For inverting the Hessian, which is a strongly banded matrix (See Figure 10), we use a simple Gauss algorithm slightly modified for taking into account all the zero-elements of the matrix.

The conjugate gradient method uses a family of $\mathbf{H}$-conjugated vectors (two vectors $\mathbf{u}$ and $\mathbf{v}$ are $\mathbf{H}$-conjugated if $\mathbf{u}^T\mathbf{H}\mathbf{v} = 0$ with $\mathbf{H}$ a symmetric positive definite matrix) to look iteratively for the solution to the system $\mathbf{H}\mathbf{h} + \mathbf{F} = 0$. In the non-linear method, the matrix $\mathbf{H}$ is recalculated during the process, while the linear method keeps it constant.

The steepest descent and the line search use the force as a search direction (The force is the opposite of the gradient, and thus indicate the direction of the steepest descent). Both methods look for a coefficient α such that $\mathbf{X_{new}} = \mathbf{X_{old}} + \alpha\mathbf{F}$ has a minimum energy. In the case of the steepest descent, the Hessian is used to approximate $E(\alpha) = E(\mathbf{X_{new}}(\alpha))$ by a parabola and finding its minimum, which is found for $\alpha = \frac{\mathbf{F}^T\mathbf{F}}{\mathbf{F}^T\mathbf{H}\mathbf{F}}$. The linear search uses decreasing powers of 2 ($\alpha = \frac{1}{2^k}$) until it finds a solution with a lower energy.

7 Integration in a Virtual Reality environment

The simulation is integrated in the Virtual Reality software *veo* of DaimlerChrysler Research and Technology. It provides the whole environment for the simulation, such as graphics, scenes and objects handling. The cable is represented as a sequence of spheres and cylinders. The spheres are set at the discretization points. The cylinders are set along the segments joining two consecutive points. The cylinders and spheres can be moved (in the geometrical limits permitted by the simulation) easily by selecting them and moving them for example with a spacemouse. At each frame, the simulation checks whether the eventually selected objects in the scene correspond to a part of a cable. If yes, its new position and orientation are taken into account, the simulation calculates the new solution and the new positions and orientations of all the spheres and cylinders are passed to the Virtual Reality software for the graphical representation.

A seamless integration into the processes already in place is necessary for the users. The data from the construction - usually in CATIA - are tessellated and converted automatically to the OpenInventor format, used for the Virtual Reality application. We also have an interface that allows to convert all or part of a tessellated wire

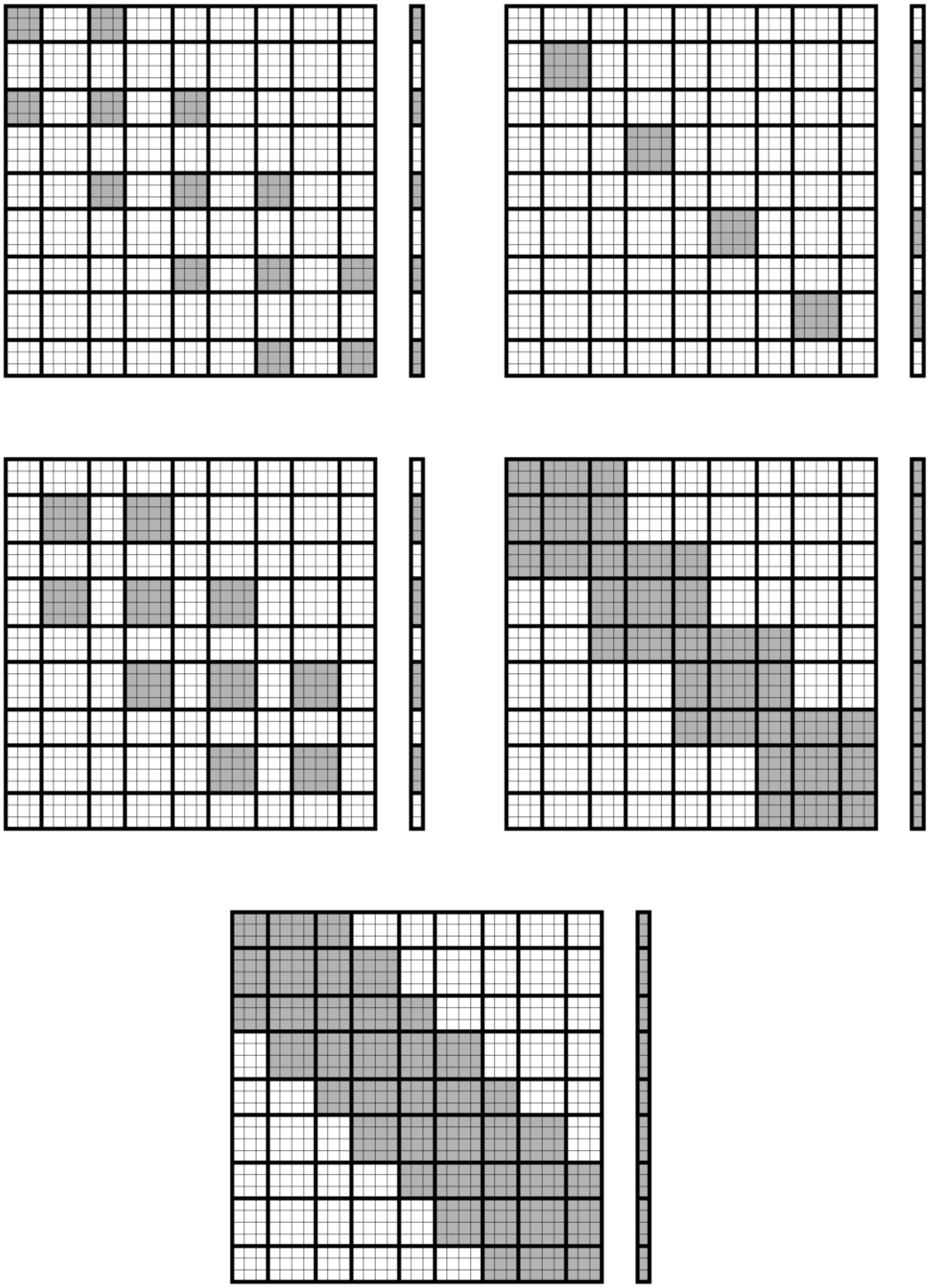

Fig. 10. Structure of the Hessian matrix and of the force vector: Represented here for $n = 5$ are the non-zero elements of the Hessian and of the force vector for the length conservation (top left), the norm of the quaternion (top right), the bending and curvature (center left) and the coherence (center right) as well as the global structure with all interactions (bottom). The banded structure of the Hessian is apparent.

harness or hose to a flexible one having the same characteristics (like length, radius, position...). A partial conversion is useful since some of the construction parts represent a huge harness that extends through the whole vehicle. The connectivity information of the tessellation triangles is parsed to create a graph representing the interconnections of the vertices. Geometrical considerations allow to find cross-sections on the surface at a given point that we use for cutting the tree at the appropriate vertices and for calculating the coordinates of points on the centerline, from which we construct the new flexible object. A copy of the tessellation with the remaining points is also created for the graphical representation. The user can also create a complete new cable between two points of the scene.

A graphical user interface groups the commands that are useful for the simulation. (See Figure 11) The simulation can be turned on or off, handles can be added or removed at selected points or can be set equidistant automatically along the cable, geometrical parameters like the radius or the length and material parameters like the Young's modulus and the Poisson coefficient can be changed interactively, the new centerline of the cables can be exported to CATIA via the VDA-FS (*Verband der Automobileindustrie - FlächenSchnittstelle*) format and can then be used as a draft for the construction. Our tool has already been tested by pilot users who have reacted positively to the possibilities offered to them.

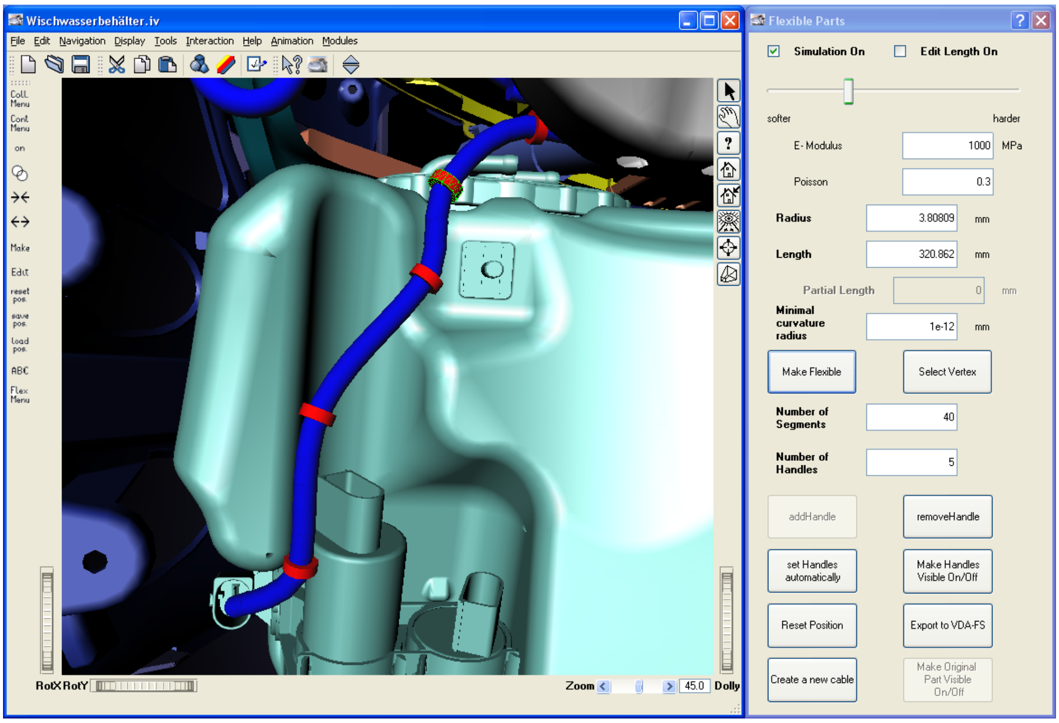

☑ Simulation On ☐ Edit Length On

E- Modulus	1000	MPa
Poisson	0.3	
Radius	3.80809	mm
Length	320.862	mm
Partial Length	0	mm
Minimal curvature radius	1e-12	mm
Number of Segments	40	
Number of Handles	5	

Fig. 11. The Graphical User Interface

The tool is used in two main contexts: assembly simulations and cable routing. In assembly simulations, flexible parts like cables or hoses are often in the way for mounting another part of the vehicle. The idea is to make the problematic part flexible (which was represented before as a rigid body), push it out of the way as it could be done with the physical parts and continue with the assembly simulation. For wire routing, a new path for the cable needs either to be defined from scratch and constructed or adapted to changes in the construction of other parts. The length of the cable may need to be adapted to the new form. We have two special modes for this, changing the handling of the stretch forces. In both cases, the integral forces relative to the length are removed. In the first mode, the user chooses two points on the cable between which the segments can be elongated either by pulling them or by typing the new length in a text field in the GUI. The reference length is then replaced either by the actual length of the segment or by the value of the text input. The length can then be changed smoothly from one iteration to another until the user is satisfied with the result. In the second mode, the stretch energy is set to

$$E_{Length,i} = \frac{k_{Length}}{2} L_i^2$$

with a very soft value for k_{Length}. The cable tends to stretch or to become shorter, finding automatically an optimal length for given endpoints and handles, thus allowing the user to route intuitively without worrying about the length. Playing with the ratio of k_{Length} and the bending and torsion stiffnesses make the form of the cable vary from “rather straight” to “rather bend”.

In order to simulate cable harnesses, the possibility to join several cables together has been added: the relative position and orientation of the cables at the ramification points are then preserved. These points can either be moved only when they are selected or they can also be dragged when one of the cables they are connecting is stretched. There is also the possibility to bind a cable with rigid objects, representing for example connectors or a part to which cables are connected. The connectors can be collision sensitive: the movement of the rigid part is determined by the collisions and by the distance restrictions coming from the cables. This is useful for assembly simulation where the central question is whether the length of the cables hanging from a part is sufficient for allowing it to be built in or out, and if not, how long the cables should be.

An important point is how well does the simulation reflect the reality: laser measurements of the deformation of brake hoses in different assembly positions were made. The various geometrical and material parameters were fitted to one of the measured position. The same material parameters were taken to simulate the other positions. The results can be seen in Figure 12. The good fitting should not hide the fact that real hoses and cables have a very high variability, depending for example on which position of a roll the hoses were stocked during fabrication: the different radii induce a rest curvature which modifies the shape of the hose. Another source of variability are the connectors: a rotation of the connector around the axis of the hose leads to a supplementary torsion. The design engineers count with a variability of one diameter.

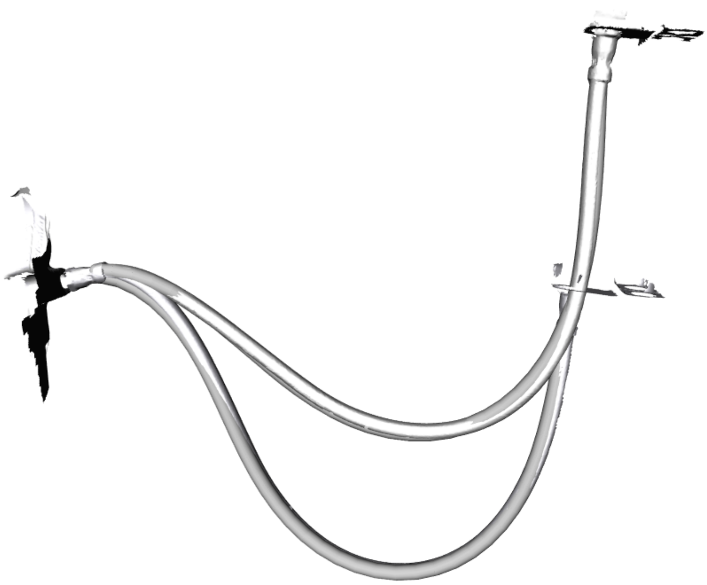

Fig. 12. Comparison of the simulation with measurements of a brake hose. The simulated hoses are in gray, the measured surface in white. The lower position was used to determine the material parameters.

8 Conclusion and future work

In this paper, we presented a virtual environment suitable for the simulation of cables. Our approach modeled the cable with an extended spring-mass system that was solved with an energy minimizing algorithm. The cable was modeled using the Cosserat theory, taking into account the conservation of length, the weight, the bending and the torsion. In order to easily formulate the bending and torsion interaction, we used a mixed coordinate system where each mass point had three space coordinates and the orientation of each segment was represented by a normalized quaternion. Each type of interaction was then calculated on the base of the coordinate type that is best suited: on the one hand, the length conservation and the contact forces with the positions, on the other hand the bending and torsion with the quaternions. Additionally, forces for the coherence between positions and quaternions and for the normalization of quaternions were employed.

For constraints that must be exactly enforced, like the length conservation, the coherence between positions and quaternions or the collision, we added an integral force at each point in the same direction as the proportional spring force. The system was solved for a constant value of those forces which were then updated as a function of the result. This mechanism allowed softer springs (and thus a less stiff system) while at the same time exactly enforcing the constraints.

Future work will include the extension of the functionalities of the user interface to better meet user needs, a better embedding of the collision response and an extension of the tool to also simulate other kinds of flexible parts.

References

[1] M. Buck, E. Schömer, Interactive rigid body manipulation with obstacle contacts, Journal of Visualization and Computer Animation 9 (1998) 243–257.

[2] J. Sauer, E. Schömer, A constraint-based approach to rigid body dynamics for virtual reality applications, in: Proc. ACM Symposium on Virtual Reality Software and Technology, 1998, pp. 153–161.

[3] R. Barzel, Faking dynamics of ropes and springs, IEEE Comput. Graph. Appl. 17 (3) (1997) 31–39.

[4] H. Finckh, T. Stegmaier, P. H. Planck, Numerische Simulation der mechanischen Eigenschaften textiler Flächengebilde - Gewebeherstellung, in: 3. LS-DYNA Anwenderforum 2004, Bamberg, 2004.

[5] K. Ward, F. Bertails, T.-Y. Kim, S. R. Marschner, M.-P. Cani, M. Lin, A survey on hair modeling: Styling, simulation, and rendering, IEEE Transactions on Visualization and Computer Graphics (TVCG) 13 (2) (2007) 213–234.
URL `http://www-evasion.imag.fr/Publications/2006/WBKMCL06`

[6] N. Magnenat-Thalmann, S. Hadap., State of the art in hair simulation, in: International Workshop on Human Modeling and Animation, Korea Computer Graphics Society, 2000, pp. 3–9.

[7] B. Thomaszewski, M. Wacker, Bending Models for Thin Flexible Objects.

[8] D. K. Pai, Strands: Interactive simulation of thin solids using Cosserat models., Comput. Graph. Forum 21 (3) (2002) 347–352.

[9] E. Hergenroether, P. Daehne, Real-time virtual cables based on kinematic simulation, in: Proceedings of the WSCG 2000, 2000.

[10] A. Loock, E. Schömer, A virtual environment for interactive assembly simulation: From rigid bodies to deformable cables, in: 5^{th} World Multiconference on Systemics, Cybernetics and Informatics (SCI'01), Vol. 3, 2001, pp. 325–332.

[11] D. Baraff, A. Witkin, Large steps in cloth simulation, in: SIGGRAPH '98: Proceedings of the 25th annual conference on Computer graphics and interactive techniques, ACM Press, New York, NY, USA, 1998, pp. 43–54.

[12] W. Schotte, Simulation des dynamischen verhaltens von kabeln für einbau-montage-simulation in vr, Master's thesis, Technische Universität Darmstadt (2005).

[13] C. A. Adrien Theetten, Laurent Grisoni, B. Barsky, Geometrycally exact dynamic splines, Tech. rep., INRIA (November 2006).

[14] J. Brown, Real-time soft tissue and suture simulation, Ph.D. thesis, Computer Science, Stanford University (November 2003).
URL
http://biocomp.stanford.edu/people/joel/MyPapers/Thesis/joelthesis.pdf

[15] V. G. A. Goss, G. H. M. van der Heijden, J. M. T. Thompson, S. Neukirch, Experiments on snap buckling, hysteresis and loop formation in twisted rods, Experimental Mechanics 45 (2005) 101–111.

[16] F. Bertails, B. Audoly, B. Querleux, F. Leroy, J.-L. Lévêque, M.-P. Cani, Predicting natural hair shapes by solving the statics of flexible rods, in: J. Dingliana, F. Ganovelli (Eds.), Eurographics (short papers), Eurographics, 2005.
URL http://www-evasion.imag.fr/Publications/2005/BAQLLC05

[17] F. Bertails, B. Audoly, M.-P. Cani, B. Querleux, F. Leroy, J.-L. Lévêque, Super-helices for predicting the dynamics of natural hair (2006) 1180–1187.

[18] M. Moll, L. E. Kavraki, Path planning for deformable linear objects, IEEE Transactions on Robotics 22 (4) (2006) 625– 636.

[19] S. S. Antman, Nonlinear Problems of Elasticity, Vol. 107 of Applied Mathematical Sciences, Springer Verlag, 1995.

[20] M. B. Rubin, Cosserat Theories: Shells, Rods and Points, Kluwer Academic Publ., Dordrecht,, 2000.

[21] W. H. Press, S. A. Teukolsky, W. T. Vetterling, B. P. Flannery, Numerical Recipes in C: The Art of Scientific Computing, Cambridge University Press, New York, NY, USA, 1992.